



Application of radial basis neural network to transform viscoelastic to elastic properties for materials with multiple thermal transitions

Xianbo Xu^{1,*} and Nikhil Gupta¹

¹ Composite Materials and Mechanics Laboratory, Mechanical and Aerospace Engineering Department, Tandon School of Engineering, New York University, Brooklyn, NY 11201, USA

Received: 1 November 2018

Accepted: 21 February 2019

Published online:

25 February 2019

© Springer Science+Business Media, LLC, part of Springer Nature 2019

ABSTRACT

Dynamic mechanical analysis is a method to characterize the frequency domain viscoelastic properties including storage and loss moduli. Methods have been developed to transform these properties to time domain and extract elastic modulus over strain rates, which is useful in mechanical design. However, application of these methods becomes increasingly complex for materials containing multiple thermal transitions. Neural networks can provide advantages in solving such problems. As the form of radial basis neural network satisfies the form obtained from time–temperature superposition principle, it is used in the present work with back-propagation to establish the master relation of loss modulus. The influence of regulation factor and neuron number is investigated to find the best parameter set. Then, storage modulus is divided into frequency-dependent and frequency-independent part. Both parts are individually calculated from loss modulus using Kramers–Kronig relation. The linear integral relation of viscoelasticity can transform the storage modulus into time-domain relaxation modulus, which can predict the stress response with specific strain history and temperature. The transformation is tested on ethylene–vinyl acetate. The time-domain elastic properties are extracted and compared with those from tensile tests at room temperature. The transformation achieves an average root mean square error of 3.3% and a maximum error 4.9% between strain rates 10^{-6} to 10^{-2} s^{-1} . This process can predict the properties at a wide range of temperatures and frequencies from a single specimen and can be implemented using parallel computing, which is promising for complex material systems.

Address correspondence to E-mail: xx579@nyu.edu

Introduction

Dynamic mechanical analysis (DMA) method has been extensively used for characterizing viscoelastic properties of polymers [1, 2], composites [3, 4] and biomaterials [5, 6]. In this method, a sinusoidal loading cycle is applied and the storage (E') and loss (E'') moduli are calculated from the in-phase and out-of-phase components of load and displacement cycles [7, 8]. The sinusoidal loading can be applied at different frequencies and temperatures, and the entire dataset can be generated on a single specimen. However, both E' and E'' are in frequency domain and do not have much significance in mechanical design field. Recent studies have focused on developing methods to transform this frequency domain data to time domain [9–11]. The time-domain data can be used to extract elastic modulus over a range of strain rates and temperatures, which has tremendous importance in engineering fields, especially for designing structures for dynamic loading conditions that can be subjected to different temperatures. Extracting the elastic modulus over a range of strain rates and temperatures from the DMA results of a single specimen eliminates the need to conduct a large number of tensile tests [12–14]. The predictions of this transform have been validated with data on neat polymers [9, 15], nanocomposites [16] and hollow particle-filled composites [10]. The method works by first applying the classic time–temperature superposition principle (TTS) to build the master curve for E' . This master curve is represented by an equation called master relation, which provides a relation for E' with respect to frequency and temperature. It allows extrapolating the values beyond the frequency range covered in the DMA experiments [17]. Then, E' is transformed to time-domain relaxation modulus $E(t)$ using linear integral relation of viscoelasticity [9, 10]. Finally, $E(t)$ is used to predict the stress response with certain strain history and temperature and obtain the elastic modulus with respect to strain rate and temperature [18].

Although the existing transformation method based on storage modulus has many advantages [11, 19, 20], it also has some limitations. First, the equations are set up for transforming data that show only one thermal transition peak in the DMA response. When more than one thermal transitions are present in the storage modulus, the current transformation methods find it difficult to identify

and model each transition, especially if two transition are close to each other. Loss modulus is able to resolve the thermal transitions better, and an approach based on loss modulus is expected to be more robust. The difficulties increase with the number of transitions. In addition, the method becomes computationally expensive because a large number of constants need to be determined to solve the equations. Use of artificial neural network (ANN) with parallel computing may have significant benefits for developing a generalized solution for this problem. A method for developing ANN-based solution for a single thermal transition material has been demonstrated [20]. However, a generalized method demonstrating the possibility of treating complex material behaviors has not been tested. Inspired by biological neural networks, ANN is efficient at handling complex nonlinear behaviors and has a strong physical foundation for use in the materials science field [21]. ANN has been used in prediction [22–24] and optimization [25] of material properties.

The master relation defined with respect to temperature and frequency is used to develop the scheme for extracting elastic modulus [19]. Using temperature and frequency as the inputs, the form of the radial basis neural network (RBNN) satisfies the form of the TTS principle and enables massive computation tasks robustly [26]. Using E'' as output, the neural network can easily identify and model each thermal transition, even though the two thermal transitions are close to each other. The E' of both strain rate sensitive and insensitive material can be divided into frequency-dependent and frequency-independent parts. Both parts can be calculated separately from E'' using Kramers–Kronig (K – K) relation [11, 27]. The properties of strain rate sensitive material are mainly contributed by the frequency-dependent part, while the properties of strain rate-insensitive material are mainly contributed by the frequency-independent part. By modeling both frequency-dependent and frequency-independent part separately, this work builds a general description of strain rate sensitive and insensitive material. It is noted that E' has a strong dependence on temperature. It will have poor fitting results when using least square error, which is the most popular one, as the object function. In addition, it is sometimes not easy to distinguish multiple thermal transitions present in the material behavior in the storage modulus curve. Hence, the scheme in the present work relies on using

loss modulus E'' , which varies in a smaller range than E' and is capable of generating better fitting results when using least square error as the object function.

The RBNN is used in the present work to build the master relation over a wide range of temperatures and frequencies. The RBNN is tested at various regulation factors and neuron numbers to find the best fitting parameters. The data are used to predict the elastic modulus of the material over a range of strain rates and temperatures. It is worth mentioning that this work is focused on building the relations between the properties obtained from different testing methodologies. Since the parameters such as materials inhomogeneity and materials quality should affect the results obtained from both testing methods, DMA and tensile tests, in a similar manner, these materials related factors are not the focus of the present study.

Materials and methods

RBNN methodology and back propagation

The two components of complex modulus, E' and E'' , are not independent, and their relation is discussed in section “Relations between storage and loss modulus”. The frequency range of master relation needs to be wide enough to implement the transformation. To build a master relation which can describe both strain rate sensitive and insensitive material behaviors under a wide range of temperatures and frequencies, E' is divided into the frequency-dependent and frequency-independent parts. The master relation of E' can be established by finding both parts individually using K – K relation. The transformation procedure is shown in Fig. 1.

The RBNN is used to establish the master relations of E'' . The frequency and temperature are chosen as the inputs of the RBNN. For multiple-layer RBNN, the mapping function between two layers can be mathematically defined as [28]

$$E(x) = \sum_{m=1}^N \beta_m \Phi_m(\|x - R_m\|) \tag{1}$$

where $E(x)$ is the output E'' , x is the vector of the input (ω and T), N is the number of basis and β_m is the coefficient of basis Φ_m . R_m is the set of centers, which is the center set of thermal transition in this work. The contribution of each basis is determined by

the distance to each basis center. The basis function is developed using the K – K relation and TTS principle. The contribution of m th neuron in the hidden layer, z_m , can be expressed by

$$z_m = \Phi_m(\alpha_m^T x - \alpha_{m0}) \tag{2}$$

where α_m is the weight vector of x and α_{m0} is the biased term for m th neuron. A three-layer RBNN is used, and it has two input neurons ω and T and one output neuron E'' . Only one hidden layer is used, and each neuron in the hidden layer corresponds to one thermal transition. The accuracy of neural network is sensitive to the neuron number and is studied in the initial part of the analysis. To reduce the over-fitting phenomenon, a regulation term $\Omega(\alpha, \beta)$ is added to the performance function as [29]

$$\tilde{F}(E''; x) = F(E''; x) + \theta \Omega(\alpha, \beta) \tag{3}$$

where α and β are the parameters of RBNN and θ is the regulation factor. Proper regulation factor needs to be chosen to achieve a balance between over-fitting and under-fitting. The mean sum of squared errors is used as the measure of error of neural network, and L^2 regulation or ridge regression is used for regulation term as

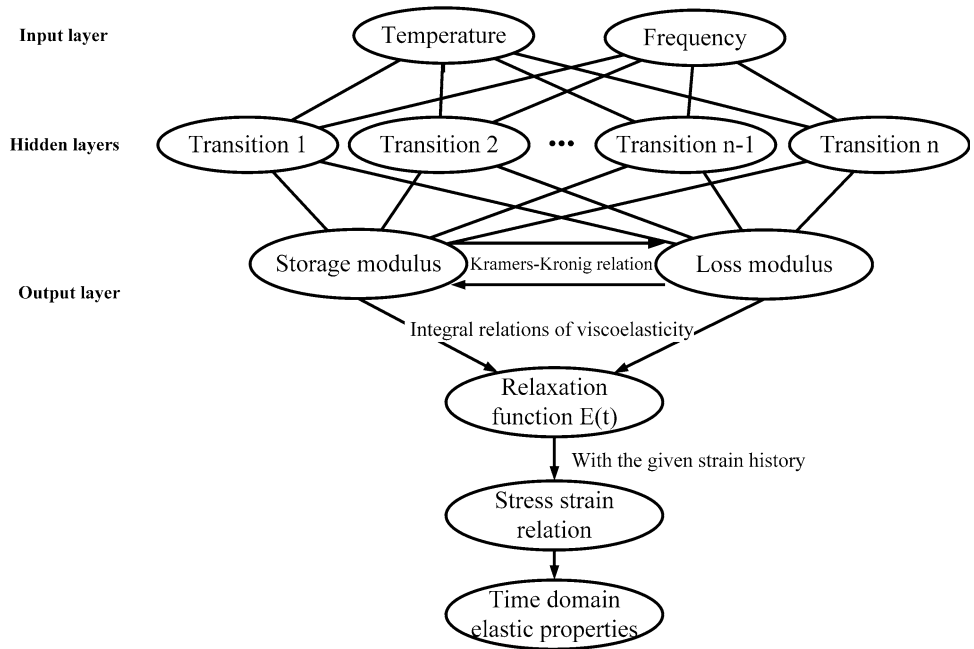
$$F(E''; x) = \frac{1}{N} \sum_{i=1}^N F_i = \frac{1}{N} \sum_{i=1}^N [E''(x_i) - \tilde{E}''(x_i)]^2 \tag{4a}$$

$$\Omega(\alpha, \beta) = \frac{1}{J} \sum_{j=1}^J a_j^2 + \frac{1}{K} \sum_{k=1}^K \beta_k^2 \tag{4b}$$

where \tilde{E}'' is the fitted loss modulus and E'' is the experimental loss modulus, F_i is the prediction error of i th data, N is the size of the dataset, J is the number of parameters between input layer and hidden layer and K is the number of parameters between hidden layer and output layer.

In order to train the RBNN, the DMA results of one specimen are used. The dataset contains the storage and loss modulus measurements at 860 combinations of temperatures and frequencies. The training process of RBNN starts by randomly dividing the dataset into training set, validation set and test set in 60:15:25 ratio. The corresponding sizes of training, validation and test set are 516, 129 and 215 data points, respectively. Then, the RBNN is trained by minimizing the performance function using training set. When the improvement in the performance diminishes, the training is stopped. The neural network is

Figure 1 The procedure of radial basis neural network modeling scheme for dynamic mechanical analysis data.



trained using back-propagation method to establish the master relation of E'' . The weights are trained to minimize the error using gradient descent, and the change of each weight for each iteration (r) can be expressed as

$$\alpha_{lm}^{(r+1)} = \alpha_{lm}^{(r)} - \gamma \left[\frac{2}{N} \sum_{i=1}^N \frac{\partial F_i}{\partial \alpha_{lm}^{(r)}} + \theta \frac{2}{J} \alpha_{lm}^{(r)} \right] \quad (5a)$$

$$\beta_m^{(r+1)} = \beta_m^{(r)} - \gamma \left[\frac{2}{N} \sum_{i=1}^N \frac{\partial F_i}{\partial \beta_m^{(r)}} + \theta \frac{2}{K} \beta_m^{(r)} \right] \quad (5b)$$

where γ is the learning rate, which is kept as 0.01; β_m is the weight between m th neuron and output; and α_{lm} is the weight between l th input and m th neuron in the hidden layer. The gradient of F can be expressed as

$$\frac{\partial F_i}{\partial \alpha_{lm}^{(r)}} = -(E''(x_i) - \tilde{E}''(x_i)) \beta_m^{(r)} x_i \Phi'_m(\alpha_m^T x_i - \alpha_{m0}) \quad (6a)$$

$$\frac{\partial F_i}{\partial \beta_m^{(r)}} = -(E''(x_i) - \tilde{E}''(x_i)) \Phi_m(\alpha_m^T x_i - \alpha_{m0}) \quad (6b)$$

The back-propagation process converges when the gradients of the weights are below 10^{-5} .

Material and experiments

The virgin EVA is of grade N8038 produced by TPI Polene, Thailand. It is injection molded into DMA and tensile test specimens at 150 °C and 60 bar. The

dimensions for DMA specimens are $60.0 \times 12.7 \times 2.5 \text{ mm}^3$ (length \times width \times height), and the geometry of tensile test specimens conforms to ASTM D638.

A TA Instruments (New Castle, DE) Q800 DMA is used to characterize the specimens in -150 to 60°C temperature range with a temperature step of 5°C . The DMA tests are conducted under dual-cantilever configuration (span length: 35 mm) with strain control mode with a maximum displacement of 25 μm . For each temperature step, the soaking time is set as 5 min to ensure thermal equilibrium. Frequency sweeps are conducted at 20 discrete frequencies logarithmically spaced between 1 and 100 Hz. The experiment is terminated when the force magnitude drops below 10^{-4} N. Three specimens are tested for repeatability. The profile of E' and E'' with respect to temperature is shown in Fig. 2 at 1 Hz frequency. The glass transition temperature is observed to be at -30°C in the material. The initial part of the graph also shows the presence of another peak at -150°C . In the previous studies, storage modulus is used for modeling the material response; however, thermal transitions are not reliably resolved in the storage modulus curve so the loss modulus is the better choice for modeling the material behavior for thermal transition temperatures. The three-dimensional response surfaces of E' and E'' are shown in Fig. 3, where both temperature and frequency sweeps are

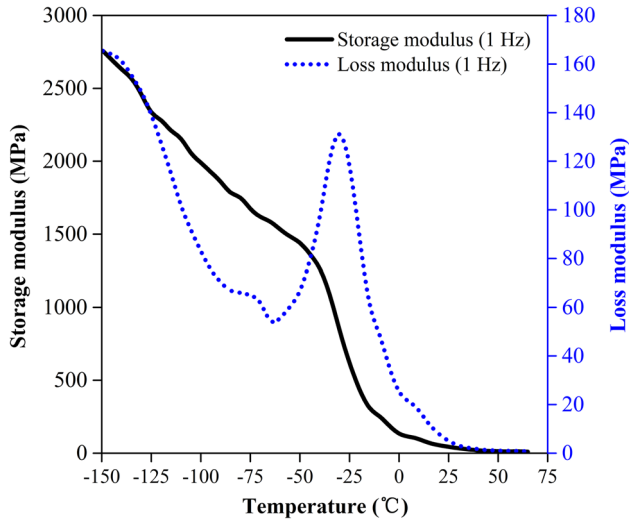


Figure 2 Profile of storage and loss moduli with respect to temperature at 1 Hz frequency.

conducted. Similar response surfaces will be plotted from the modeling results for comparison with the experimental results.

An Instron 4467 universal test system is used for the time-domain viscoelastic properties at room temperature. An Instron 25-mm gage length extensometer is used to obtain the strain history data under different initial strain rates from 2.5×10^{-6} to $2.5 \times 10^{-3} \text{ s}^{-1}$. Four specimens are repeated for each strain rate, and a representative set of stress–strain curves for EVA is presented in Fig. 4.

Relations between storage and loss modulus

The $E'(\omega)$ and $E''(\omega)$ are not independent and their relation at a given temperature T can be expressed as [30]

$$E'(\omega, T) - E'(0, T) = \frac{2}{\pi} \int_0^\infty \frac{\omega^2 E''(\lambda, T)}{\lambda(\omega^2 - \lambda^2)} d\lambda \tag{7}$$

where ω is the angular frequency and $E'(0, T)$ is the E' at frequency 0. The right side represents the difference between storage modulus at frequency 0 and ω , which can be named as $\Delta E'$. $\Delta E'$ is a function of frequency and temperature while $E'(0, T)$ is frequency-independent. Using this relation, the temperature-dependent E' can be divided into frequency-independent component $E'(0, T)$ and frequency-dependent component $\Delta E'(\omega, T)$. The $E'(0, T)$ is simplified as $E'_0(T)$ for convenience in the following work as

$$\Delta E'(\omega, T) = \frac{2}{\pi} \int_0^\infty \frac{E''(\lambda, T)\omega^2}{\lambda(\omega^2 - \lambda^2)} d\lambda \tag{8a}$$

$$E'_0(T) = E'(\omega, T) - \frac{2}{\pi} \int_0^\infty \frac{E''(\lambda, T)\omega^2}{\lambda(\omega^2 - \lambda^2)} d\lambda \tag{8b}$$

To implement this process, E'' at wide range of frequencies and temperatures needs to be found. Taking derivative with respect to ω on both sides of Eq. 8.b:

$$\frac{dE'(\omega, T)}{d \ln \omega} = \frac{d\Delta E'(\omega, T)}{d \ln \omega} = -\frac{4}{\pi} \int_0^\infty \frac{\lambda E''(\lambda, T)}{(\omega^2 - \lambda^2)^2} d\lambda \tag{9}$$

The K – K relation can be found when E'' changes slowly with ω as per the following equation [27] and can be used to find the radial basis function

$$E''(\omega, T) \approx \frac{\pi}{2} \frac{dE'(\omega, T)}{d \ln \omega} \tag{10}$$

Zeltmann et al. [9] used sigmoid function to describe E' for single thermal transition as

$$E'(\omega) = a + b \tanh(c \ln(\omega) + d) \tag{11}$$

where a, b, c and d are the parameters that need to be determined. By combining Eqs. 8 and 9, the corresponding radial basis of E'' for i th transition can be found as

$$E''(\omega) = \text{sech}^2(c \ln(\omega) + d) \tag{12}$$

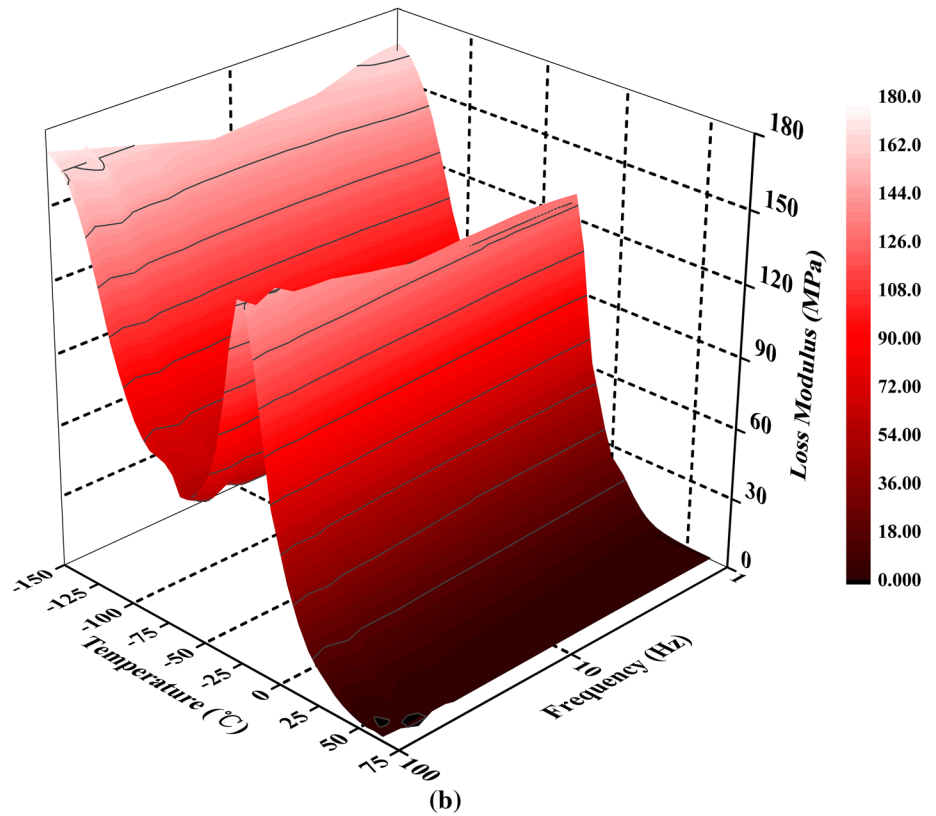
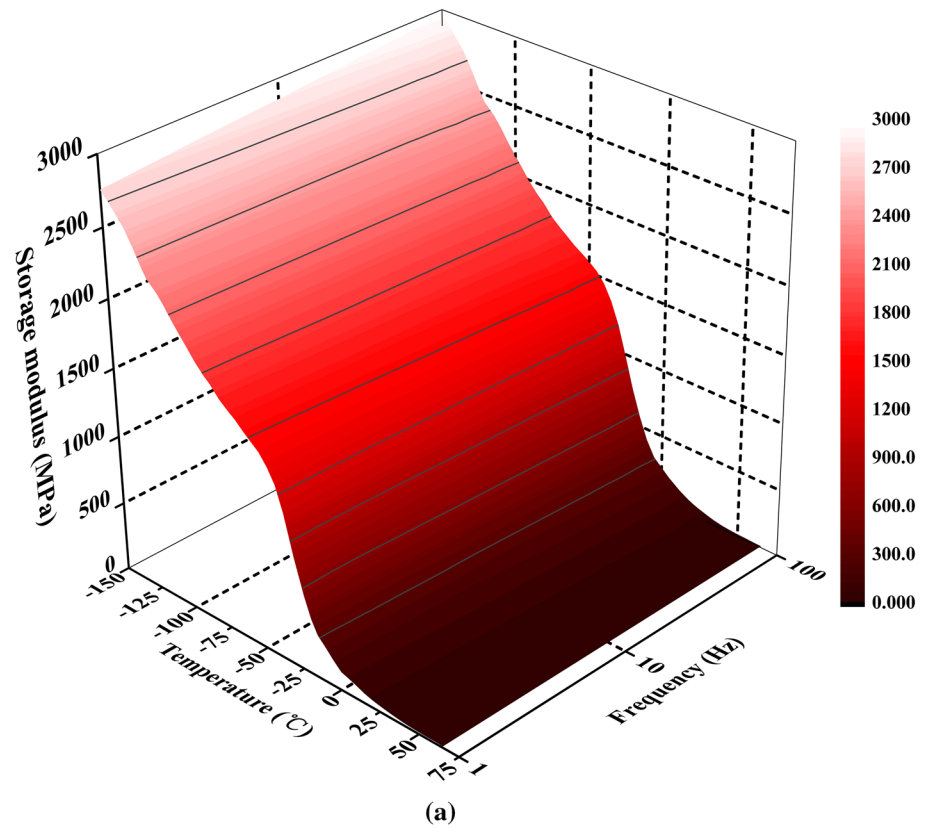
The radial basis can be expanded to temperature using TTS principle. According to TTS principle, the master relation of the instantaneous modulus does not change shape as the temperature is changed. Following TTS principle, the parameters c is constant under different temperatures and only d is a function of temperature T . The linear form is used between hidden layers and the radial basis function of E'' for i th transition can be established as

$$E''_i(\omega, T) = \text{sech}^2(c_i \ln(\omega) + d_i T + e_i) \tag{13}$$

where e_i is the bias term for each layer. The RBNN is used to establish the material relation of E'' for multiple transitions material. The neural network can be expanded to a frequency range of 10^{-50} to 10^{50} , which is large enough for Eq. 8.

The RBNN can be integrated with respect to ω to find $E'_0(T)$. It is fitted using a sigmoid function as

Figure 3 Three-dimensional (3D) response surfaces of **a** storage modulus and **b** loss modulus for EVA constructed from dynamic mechanical analysis data.



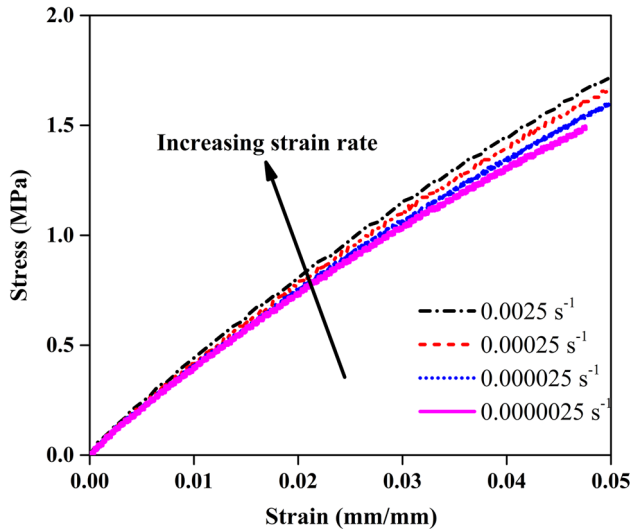


Figure 4 A representative set of tensile stress–strain curves for EVA at four different strain rates.

$$E'_0(T) = a_0 + b_0(T - T_0)_+ + w_0 \tanh(d_0 T + e_0) \tag{14}$$

where a_0 , b_0 and w_0 are parameters to fit $E'_0(T)$, $(T - T_0)_+$ is a piecewise linear function and it can be defined as

$$(T - T_0)_+ = \begin{cases} (T - T_0) & T \geq T_0 \\ 0 & T < T_0 \end{cases} \tag{15}$$

Following this method, the master relations of E' and E'' can be found, which can describe the viscoelastic relation at a wide range of frequencies and temperatures and be used for transformation to time domain.

Transform to time domain

The frequency domain master relation of E' can be transformed to time-domain relaxation function at a certain temperature T , $E(t, T)$, using integral relations of viscoelasticity as [30]

$$E(t, T) = \frac{2}{\pi} \int_0^\infty \frac{E'(\omega, T)}{\omega} \sin(\omega t) d\omega \tag{16}$$

For thermal equilibrium, the stress–strain relation with specific strain history can be found using

$$\sigma(t, T) = E * \dot{\epsilon} = \int_0^t E(t - \tau, T) \frac{d\epsilon(\tau)}{d\tau} d\tau \tag{17}$$

where σ , ϵ and τ are stress, strain and time variable, respectively. For tensile test, the strain rate is assumed to be constant and the time-dependent stress history can be approximated as [30]

$$\sigma(t, T) = \dot{\epsilon} \int_0^t E(\tau, T) d\tau \tag{18}$$

Using this transformation, the stress–strain relation can be predicted and the time-domain elastic modulus can be extracted at various temperatures and strain rates.

Results and discussion

Model tuning

As the fitting results are influenced by the penalty factors θ and neuron numbers, the modeling process consists of two steps: First, RBNN is tested by mathematical experiments to determine the best training parameters; then, the parameters are used on experimental data to establish the master relation of E' and E'' under a wide range of temperatures and frequencies.

The best training parameter is found by a mathematical experiment. A mathematical model is used to simulate the material behavior with two thermal transitions. The RBNN is trained on the simulated data to find the best parameters. The mathematical model is generated by training the RBNN using the experimental E'' without penalty factor ($\theta = 0$). The RBNN for the mathematical model has one hidden layer containing two neurons. The training, validation and test sets are generated using the mathematical model. To test the robustness of the method, two different levels of Gaussian noises are added into training set as

$$\tilde{E}'_{\text{train/validation}} = \tilde{E}'(1 + \zeta) \tag{19}$$

where ζ is a Gaussian distribution with mean of 0 and the standard deviation is set at 0.05 and 0.025. Then the RBNN is trained with different penalty factors and neuron numbers using the data generated by the mathematical model. The accuracy of RBNN is found by comparing the prediction of RBNN and mathematical model, and average training and testing

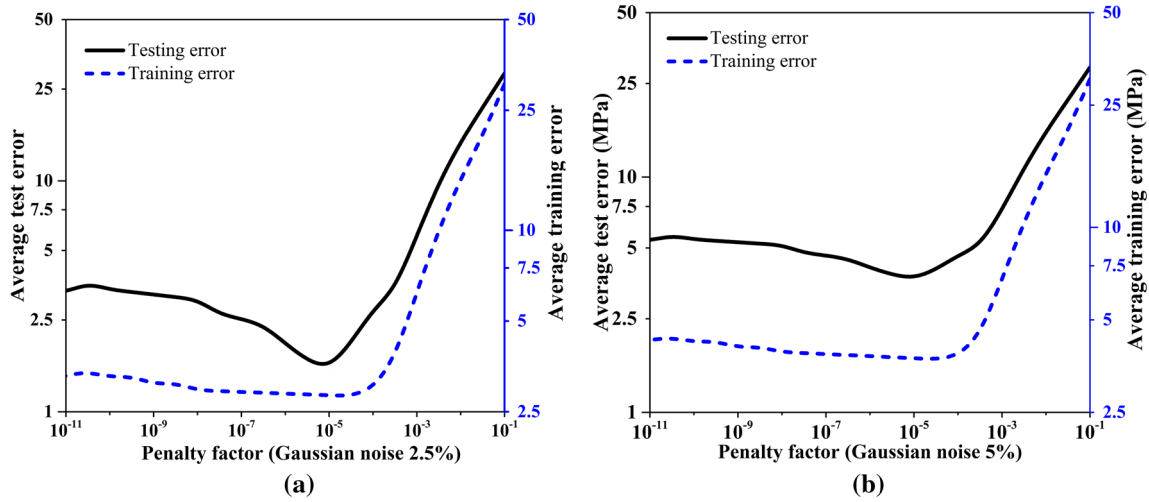


Figure 5 The training error and testing error with respect to regulation factor θ at **a** 2.5% and **b** 5% Gaussian noises (Number of neurons = 2).

errors are found using root mean square error. The experiments are repeated for 500 times to find the average training and testing errors.

The RBNN is trained in the penalty factor range of 10^{-11} to 10^{-1} . The errors with respect to penalty factor θ are shown in Fig. 5. The RBNN achieves the best accuracy when the penalty factor θ is around 10^{-5} . The under-fitting problem imperils the accuracy when the penalty factor θ is more than 10^{-3} and the penalty factor is so large that it dominates the fitting. On the contrary, the over-fitting problem appears when the penalty factor θ is less than 10^{-7} . The penalty factor is not strong enough to constrain the over-fitting and compromise the accuracy.

The trend of accuracy with respect to neuron number is also investigated. The penalty factor θ is set to be 10^{-5} and it is trained with different neuron numbers as per the results shown in Fig. 6. The RBNN achieves the best accuracy when its neuron number equals 2, which agrees with the neuron number in the mathematical model. Similar to the trend in penalty factor, the under-fitting jeopardizes the accuracy when the neuron number is less than 2 and the RBNN is not powerful enough. The accuracy decreases when the neuron number is much larger than 2 due to over-fitting.

The master relation of E'' is established using RBNN with 2 neurons and penalty factor 10^{-5} . The

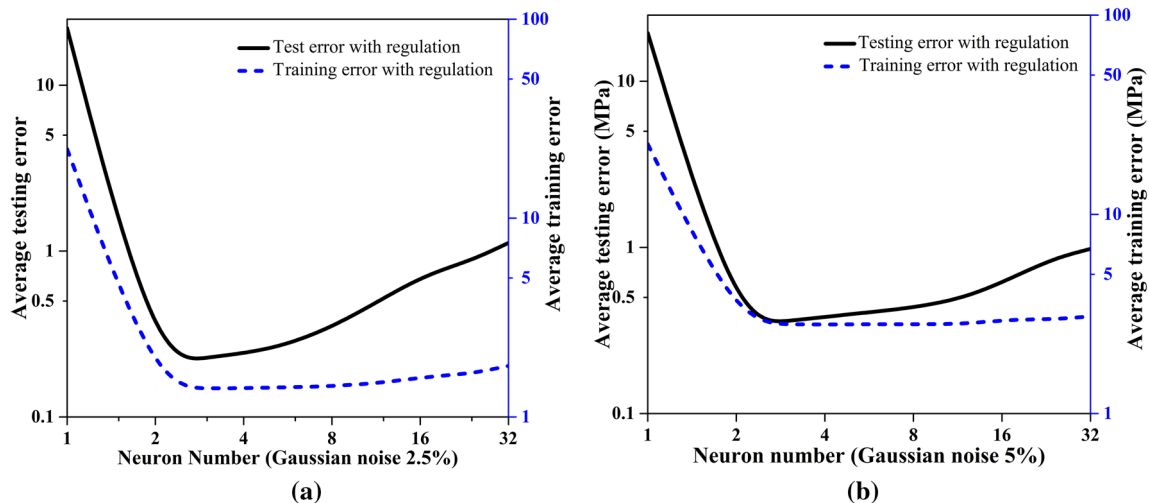
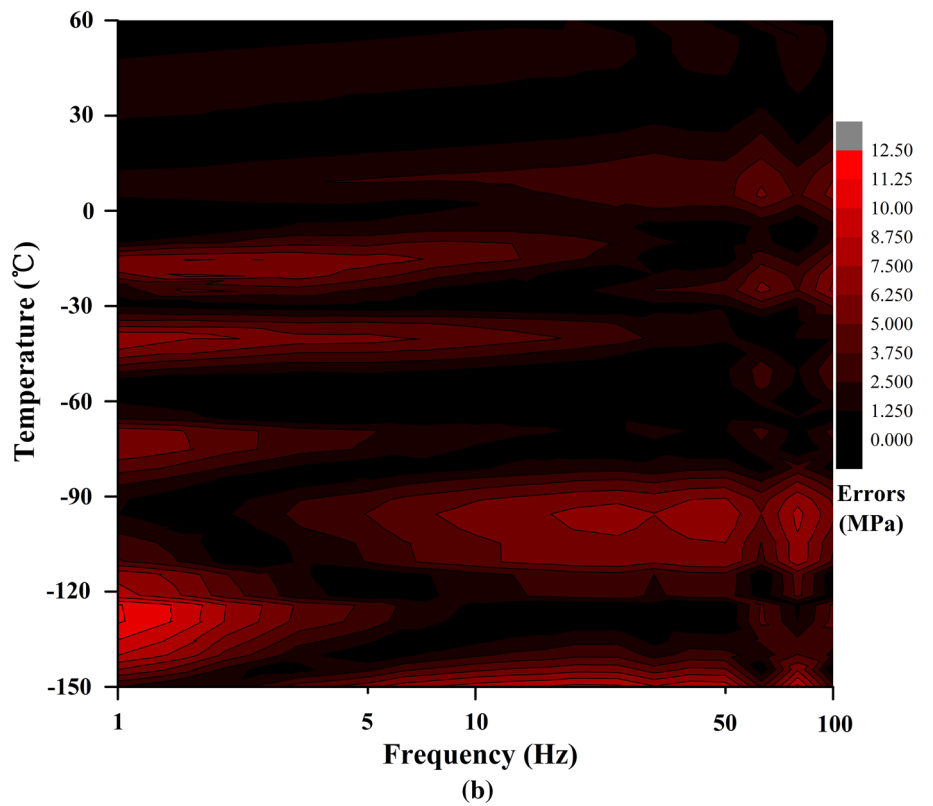
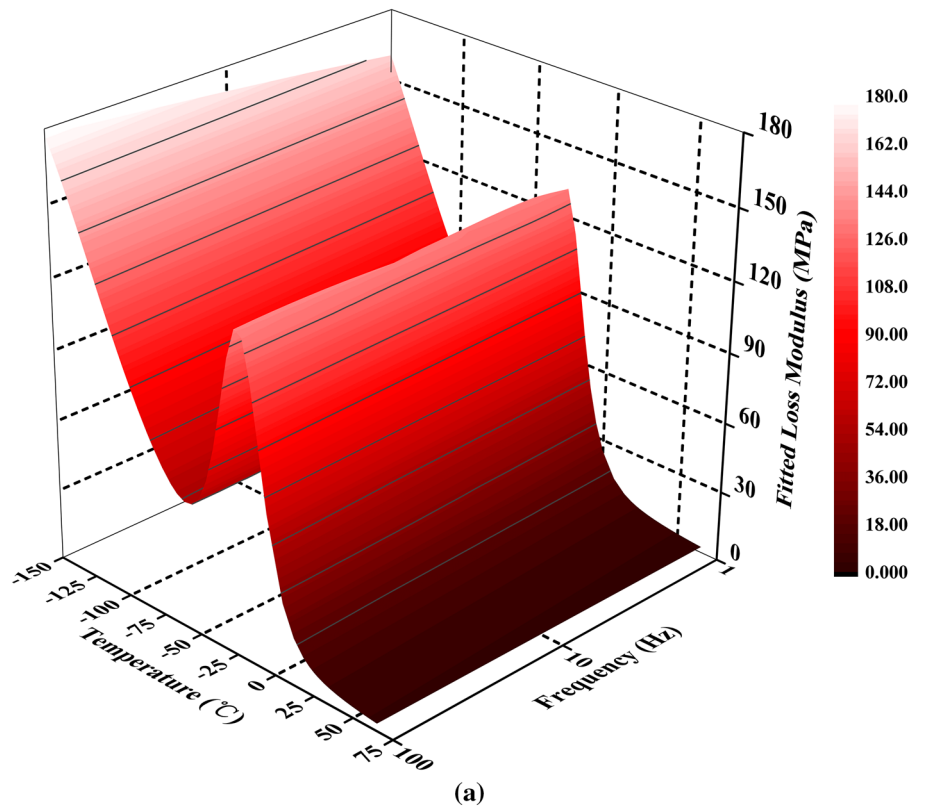


Figure 6 The training error and testing error with respect to number of neurons at **a** 2.5% and **b** 5% Gaussian noises (Regulation factor $\theta = 10^{-5}$).

Figure 7 **a** Response surface of loss modulus fitted by RBNN. **b** Map of the fitting error with respect to temperature and frequency.



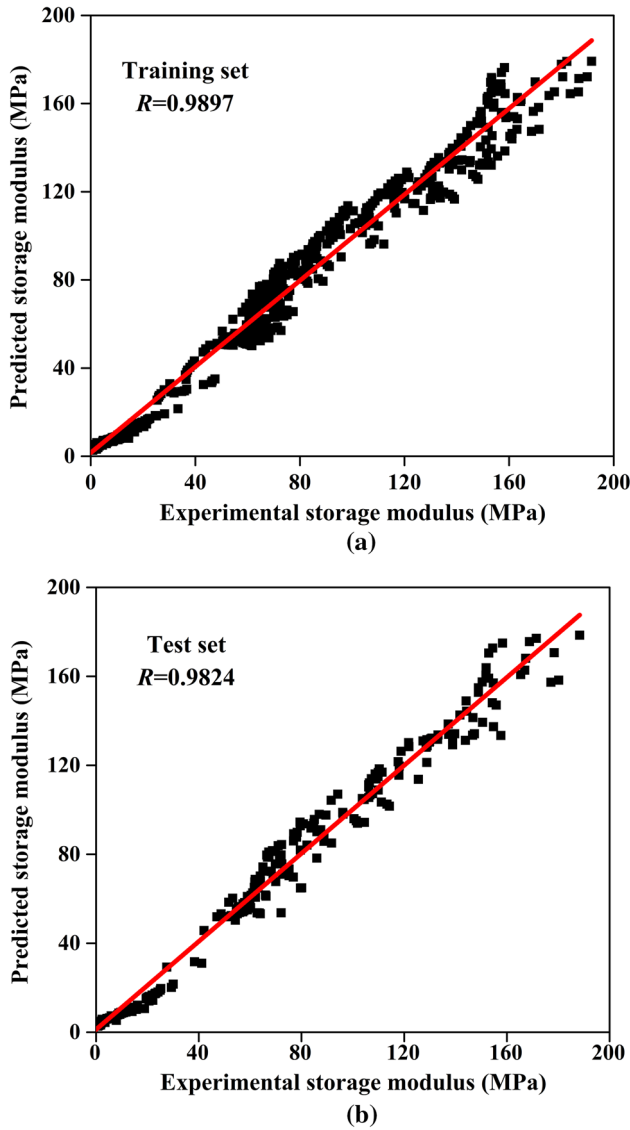


Figure 8 The Pearson's correlation coefficient R of the experimental and predicted storage modulus for **a** training set **b** test set.

average error of test set is 2.72 MPa, which is 3.89% of the average loss modulus. The response surface of predicted E'' with respect to temperature and frequency is shown in Fig. 7a, and the map of fitting error is shown in Fig. 7b. The Pearson correlation coefficient R for training set and test set is found to be 0.9897 and 0.9824, as shown in Fig. 8. The region near the thermal transition temperature, where E'' achieves the peak, shows the highest level of error. With the master relation of E'' , $\Delta E'$ and $E'(0)$ can be calculated individually. The $E'(0)$ and the fitting results are shown in Fig. 9 and show close matching

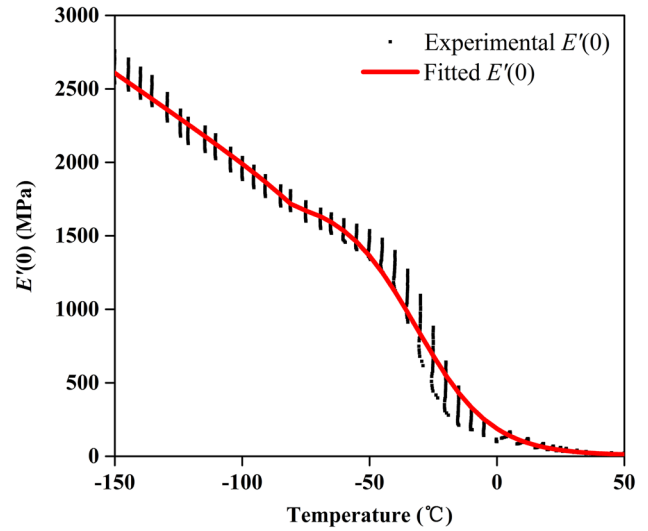


Figure 9 The frequency-independent part of storage modulus $E'(0)$.

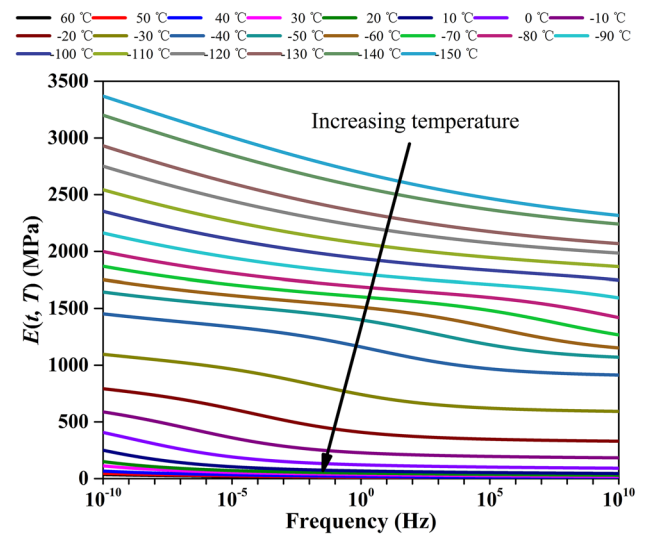


Figure 10 Time-domain relaxation modulus $E(t, T)$ with respect to frequency at different temperatures. Both increase in temperature and frequency show decrease in the relaxation modulus.

with each other at the entire temperature range. The variation of experimental $E'(0)$ is contributed by the error of E'' .

Transformation to elastic modulus

The master relation of E' can be transformed to time-domain relaxation modulus $E(t, T)$ using Eqs. 16–18. The $E(t, T)$ at different temperatures is shown in

Figure 11 Response surface of predicted elastic modulus with respect to temperature and strain rate.

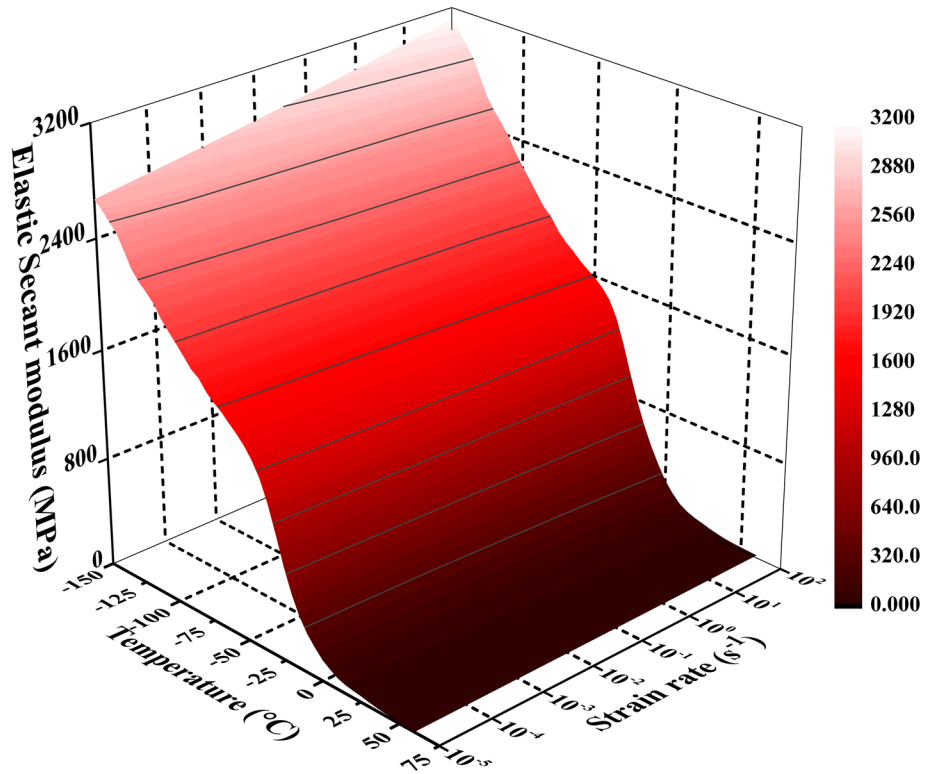


Fig. 10. Then the stress response with certain strain history under different temperatures can be extracted, which can be used to calculate the elastic modulus.

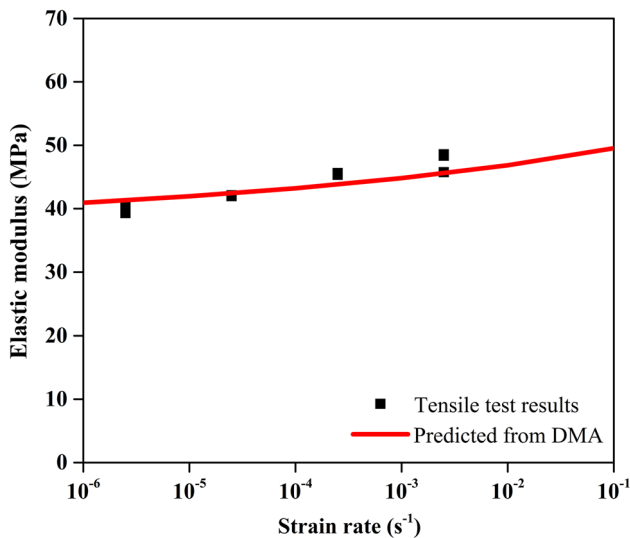


Figure 12 Comparison between predicted and experimental elastic modulus values at room temperature. Four experimental data points are plotted at each strain rate but some of them overlap due to the close values.

The elastic modulus is defined using 0.5% secant modulus due to nonlinear elastic response of EVA, and its response surface of EVA with respect to temperature and strain rates, predicted from the present model, is presented in Fig. 11. To evaluate the accuracy of transformation results, the elastic modulus obtained from the transform is compared with the experimentally measured modulus obtained from tensile test results shown in Fig. 12. Four experimental data points are plotted in this figure for each strain rate. Some of the values are very close and overlap with each other. The predictions achieve an average root mean square error (RMS) of 3.3% RMS and the maximum error is 4.9%, which affirms the applicability and accuracy of the present method.

The method can predict the elastic properties over a wide range of temperatures and strain rates from the results of DMA testing on a single specimen. It is also successful in dealing with material that has two thermal transitions in the test temperature range. A similar procedure will be applicable if there are a larger number of thermal transitions, with the possible main difference that the RBNN optimization process will result in a different parameter set for optimization. The present method eliminates the need for a large number of tensile tests. In addition,

the present scheme based on artificial neural network can be effectively implemented in parallel computing to allow transforming properties of materials that have multiple thermal transitions in the test results.

Conclusions

In this work, a method is developed to transform the frequency domain DMA testing results to time-domain elastic modulus at various temperatures and strain rates. EVA is used as the study material for this work, and RBNN is used to establish the master relations of E'' at a wide range of temperatures and frequencies. With the L^2 regulation factor, the RBNN is tested under various regulation factors and neuron numbers to find the best training parameters. Then E' is divided into frequency-dependent and frequency-independent components to build a general description of strain rate sensitive and insensitive materials with multiple thermal transitions. Two parts are individually calculated from master relations of E'' using the K – K relation and then transformed to $E(t, T)$. The $E(t, T)$ can be used to predict the viscoelastic response with certain strain history and temperature, and the elastic properties can be extracted. To verify the accuracy of the transform, the elastic modulus predicted from the DMA transform is compared with the values obtained from experimental tensile tests. At strain rate between 10^{-6} and 10^{-2} s^{-1} , the transformation achieves 3.3% RMS average error and 4.9% maximum error. Based on the RBNN, the process is easy to be implemented using parallel computing and is robust. The study focuses on the testing methodology, not on the material composition or microstructure, and the transform should work on any other material with multiple thermal transitions.

Acknowledgements

This work is supported by the Office of Naval Research N00014-10-1-0988. Dr. Mrityunjay Doddamani of NITK, Surathkal, India, is thanked for providing the EVA samples used for generating experimental results.

Compliance with ethical standards

Conflict of interest The authors declare that they have no conflict of interest.

References

- [1] Polak-Krašna K, Dawson R, Holyfield LT, Bowen CR, Burrows AD, Mays TJ (2017) Mechanical characterisation of polymer of intrinsic microporosity PIM-1 for hydrogen storage applications. *J Mater Sci* 52(7):3862–3875. <https://doi.org/10.1007/s10853-016-0647-4>
- [2] Lai J-C, Li L, Wang D-P, Zhang M-H, Mo S-R, Wang X, Zeng K-Y, Li C-H, Jiang Q, You X-Z, Zuo J-L (2018) A rigid and healable polymer cross-linked by weak but abundant Zn(II)-carboxylate interactions. *Nat Commun* 9(1):2725
- [3] Feng J, Guo Z (2016) Effects of temperature and frequency on dynamic mechanical properties of glass/epoxy composites. *J Mater Sci* 51(5):2747–2758. <https://doi.org/10.1007/s10853-015-9589-5>
- [4] Helgeson ME, Moran SE, An HZ, Doyle PS (2012) Mesoporous organohydrogels from thermogelling photocrosslinkable nanoemulsions. *Nat Mater* 11:344
- [5] Zhang Y, Nanda M, Tymchysyn M, Yuan Z, Xu C (2016) Mechanical, thermal, and curing characteristics of renewable phenol-hydroxymethylfurfural resin for application in biocomposites. *J Mater Sci* 51(2):732–738. <https://doi.org/10.1007/s10853-015-9392-3>
- [6] Lieleg O, Kayser J, Brambilla G, Cipelletti L, Bausch AR (2011) Slow dynamics and internal stress relaxation in bundled cytoskeletal networks. *Nat Mater* 10:236
- [7] Shunmugasamy VC, Pinisetty D, Gupta N (2013) Viscoelastic properties of hollow glass particle filled vinyl ester matrix syntactic foams: effect of temperature and loading frequency. *J Mater Sci* 48(4):1685–1701. <https://doi.org/10.1007/s10853-012-6927-8>
- [8] Ferry JD (1980) Dependence of viscoelastic behavior on temperature and pressure. *Viscoelastic properties of polymers*. Wiley, New York
- [9] Zeltmann SE, Bharath Kumar BR, Doddamani M, Gupta N (2016) Prediction of strain rate sensitivity of high density polyethylene using integral transform of dynamic mechanical analysis data. *Polymer* 101:1–6
- [10] Zeltmann SE, Prakash KA, Doddamani M, Gupta N (2017) Prediction of modulus at various strain rates from dynamic mechanical analysis data for polymer matrix composites. *Compos B Eng* 120:27–34
- [11] Xu X, Gupta N (2018) Determining elastic modulus from dynamic mechanical analysis: a general model based on loss modulus data. *Materialia* 4:221–226
- [12] Romero PA, Zheng SF, Cuitiño AM (2008) Modeling the dynamic response of visco-elastic open-cell foams. *J Mech Phys Solids* 56(5):1916–1943
- [13] Luong DD, Pinisetty D, Gupta N (2013) Compressive properties of closed-cell polyvinyl chloride foams at low and

- high strain rates: experimental investigation and critical review of state of the art. *Compos B Eng* 44(1):403–416
- [14] Peroni L, Scapin M, Fichera C, Lehmkus D, Weise J, Baumeister J, Avallè M (2014) Investigation of the mechanical behaviour of AISI 316L stainless steel syntactic foams at different strain-rates. *Compos B Eng* 66:430–442
- [15] Koomson C, Zeltmann SE, Gupta N (2018) Strain rate sensitivity of polycarbonate and vinyl ester from dynamic mechanical analysis experiments. *Adv Compos Hybrid Mater* 1(2):341–346
- [16] Xu X, Koomson C, Doddamani M, Behera RK, Gupta N (2019) Extracting elastic modulus at different strain rates and temperatures from dynamic mechanical analysis data: a study on nanocomposites. *Compos B Eng* 159:346–354
- [17] Jia Z, Amirkhizi AV, Nantasetphong W, Nemat-Nasser S (2016) Experimentally-based relaxation modulus of polyurea and its composites. *Mech Time-Dependent Mater* 20(2):155–174
- [18] Lin KSC, Aklonis JJ (1980) Evaluation of the stress-relaxation modulus for materials with rapid relaxation rates. *J Appl Phys* 51(10):5125–5130
- [19] Xu X, Gupta N (2018) Determining elastic modulus from dynamic mechanical analysis data: reduction in experiments using adaptive surrogate modeling based transform. *Polymer* 157:166–171
- [20] Xu X, Gupta N (2019) Artificial neural network approach to predict the elastic modulus from dynamic mechanical analysis results. *Adv Theory Simul*. <https://doi.org/10.1002/adts.201800131>
- [21] Butler KT, Davies DW, Cartwright H, Isayev O, Walsh A (2018) Machine learning for molecular and materials science. *Nature* 559(7715):547–555
- [22] Ning L (2009) Artificial neural network prediction of glass transition temperature of fluorine-containing polybenzoxazoles. *J Mater Sci* 44(12):3156–3164. <https://doi.org/10.1021/ci010062o>
- [23] Lin YC, Fang X, Wang YP (2008) Prediction of metadynamic softening in a multi-pass hot deformed low alloy steel using artificial neural network. *J Mater Sci* 43(16):5508–5515. <https://doi.org/10.1007/s10853-008-2832-6>
- [24] Shabani MO, Mazahery A (2011) Modeling of the wear behavior in A356–B4C composites. *J Mater Sci* 46(20):6700–6708. <https://doi.org/10.1007/s10853-011-5623-4>
- [25] Malho Rodrigues A, Franceschi S, Perez E, Garrigues J-C (2015) Formulation optimization for thermoplastic sizing polyetherimide dispersion by quantitative structure–property relationship: experiments and artificial neural networks. *J Mater Sci* 50(1):420–426. <https://doi.org/10.11648/j.am.20150704.14>
- [26] Dey P, Gopal M, Pradhan P, Pal T (2017) On robustness of radial basis function network with input perturbation. *Neural Comput Appl*. <https://doi.org/10.1007/s00521-017-3086-5>
- [27] Booij HC, Thoone GPJM (1982) Generalization of Kramers-Kronig transforms and some approximations of relations between viscoelastic quantities. *Rheol Acta* 21(1):15–24
- [28] Dorffner G (1992) EuclidNet—a multilayer neural network using the euclidian distance as propagation rule. In: Alexander I, Taylor J (eds) *Artificial neural networks*. North-Holland, Amsterdam, pp 1633–1636
- [29] Goodfellow I, Bengio Y, Courville A (2016) *Deep learning*. Adaptive computation and machine learning series. The MIT Press, Cambridge
- [30] Christensen RM (1982) *Theory of viscoelasticity: an introduction*. Dover Civil and Mechanical Engineering, 2nd edn. Academic Press, New York

Publisher's Note Springer Nature remains neutral with regard to jurisdictional claims in published maps and institutional affiliations.